Supplementary Materials for

Accurate Concentration Control of Mitochondria and Nucleoids

Rishi Jajoo, Yoonseok Jung, Dann Huh, Matheus Viana, Susanne Rafelski, Michael Springer and Johan Paulsson

correspondence to: johan_paulsson@hms.harvard.edu

This PDF file includes:

Materials and Methods
Supplementary Text
References (28-38)
Figs. S1 to S16
Table S1

Materials and Methods

Nucleoid Counting Assay

We developed a novel assay for counting individual mitochondrial nucleoids in single dividing cells: live *S. pombe* stained by Sybr Green I (SGI) showed clear puncta resembling mitochondrial nucleoids, had no detectable signal in the nucleus and had minimal autofluorescence (Fig. S4A). These SGI puncta co-localized with a mitochondrial matrix-targted mCherry fluorophore, and were not observed in cells lacking mtDNA (ρ^0, Fig. S5B). To verify that SGI puncta were nucleoids, we co-stained cells with a previously used nucleoid stain, DAPI *(28)* and saw a close correspondence between individual nucleoids identified by each method. Using a semi-automated image analysis method to count the number of nucleoids stained (see below), we also found that the average number of nucleoids detected by each method was nearly identical (Fig. S4B). This procedure produces two estimates for each individual cell, and we found that, on average, the low estimate was approximately 92% of the high estimate. To account for the fact that both methods then slightly undercount nucleoids, we performed a more rigorous statistical analysis showing that each nucleoid is independently detected with an efficiency of about 84% with either stain (Fig. S6).

Estimation of detection efficiency from DAPI and SGI staining

To estimate the staining efficiency of DAPI and SGI, each cell as assumed to have some number of nucleoids, N, and each stain was assumed to detect individual nucleoids with a probability, p. This probability was assumed to be the same for each stain as the slope of the best fit line between them was 1.0. For each cell, the average number of spots detected via DAPI and SGI was used as an estimate for Np. All cells with the same number of average detected nucleoids were grouped and the individual samples were treated as binomial process with N trials, each with p chance of success. The variance of this process is $Np(1-p)$ and p was computed by assuming that the average number of detected nucleoids for the group was Np. The result from each of these groups of cells was averaged with weight proportional to the number of samples and resulted in the estimated 84% detection efficiency.

Estimation of detection efficiency from EdU staining

To further validate SGI staining we compared it to cells where nucleoids were labeled with the nucleotide analog 5-ethynyl-2'-deoxyuridine (EdU), followed by ``click" ligation of Alexa-488 azide (see below). EdU labels nucleoids reliably *(16)* but only in fixed cells after a cell cycle arrest (Fig. S7A) and thus can only be used for assay validation purposes. In a matched population of cells, SGI stained approximately 84% of nucleoids stained by EdU (Fig. S7B), agreeing with our previous estimate of labeling efficiency. SGI staining is therefore an accurate method for quantifying nucleoid numbers in single cells, but has two significant limitations: the experimental procedure disrupts the native localization of mitochondria and nucleoids, and nucleoids do not remain labeled if cells resume growth. Therefore, this assay cannot be used to monitor nucleoid position or number over time or in space. However, it does allow us to count the number of nucleoids in each daughter of dividing cells, and when combined with judiciously chosen

cell division mutants, can be used to identify key properties of the nucleoids segregation process.

Correction for Detection Efficiency of Nucleoids

The observed segregation errors indicate that nucleoids partition to daughter cells more accurately than a binomial model However, we wanted to ensure that this result held true even though we detected only ~80-90% of nucleoids. Huh and Paulsson showed that unbiased incomplete detection would make the data look more like binomial segregation than it actually is *(7)* Because we observed better than binomial segregation without any corrections, this would imply nucleoids are actually even more accurately segregated when the imperfect detection is accounted for.

To quantitatively correct for detection error of nucleoids, we use equation S81 of Huh and Paulsson *(7)* If l and r represent the number of nucleoids detected in the left and right cells respectively, L and R are the number actually in the left and right cells, and u is the efficiency of detection, then the conversion between the average squared error observed and the average squared error actually present is

$$\frac{1}{u^2}\left[\left\langle (l-r)^2\right\rangle + (u-1)\left\langle l+r\right\rangle\right] = \left\langle (L-R)^2\right\rangle$$

The result of correcting the observed data in this way is shown in Figure S11. It shows that the nucleoid segregation is likely even more accurate than we observed. We plotted the uncorrected data in Figure 2 of the main text as a conservative estimate of the error in segregation.

Estimation of concentration errors during segregation

Nucleoid partitioning may in fact be significantly more accurate than it appears in our experiments. The measured relative nucleoid concentration noise between sister cells is 18%. This is a slight over-estimate due to the under-counting statistics explained above. In addition, we estimated the cytoplasmic volume of the cell assuming it is occupied only by nuclei constituting exactly 11% of the cell volume. In reality, the size of the nucleus varies *(29)* and other structures such as vacuoles, ER and golgi etc. displace cytoplasm and introduce noise into the estimate of the cytoplasmic volume. Since we find that mitochondria segregate in proportion to the available volume (e.g. the fit to ``equal concentration'' is better when we exclude the volume of the nucleus), we are likely overestimating the amount of concentration noise introduced at cell division.

For comparison, a mechanism that divides exactly half of the nucleoids in each daughter cell would have concentration errors of 10% between cells. Such a high error from a ``perfect'' mechanisms arises because daughter cells differ in size on average by 5% and when there are an odd number of nucleoids in a cell, they must be divided unevenly. Therefore, accounting for errors in measurement might indicate that the segregation of mitochondrial nucleoids is actually more accurate than a ``perfect'' mechanism.

On the other hand, if nucleoids segregated by a binomial mechanism with inheritance proportional to the cell volume of each daughter cell, the concentration error of nucleoids between daughter cells would be 29%.

Sybr Green I and DAPI staining

All cultures were grown in YES media with 4% glucose at 30° C before staining experiments. Overnight cultures were diluted approximately 100 to 1000-fold, allowed at least 2 doublings and grown to OD600 ~0.1. Approximately 1mL of culture was spun at 3000g for 1 minute and washed with 1x PBS. Volume was brought up to 100 uL (PBS) and 0.5 uL of Sybr Green I (Life Technologies, S-7567) (undiluted from stock) and/or DAPI (Sigma-Aldrich, D9542) (5 ug/uL) was added and contents were gently mixed. Cells were then immediately spun (as above) and washed with PBS twice before imaging.

EdU Staining

For EdU incorporation into strains yFS284 and RJP028, strains were grown from overnight cultures at 27° C and then diluted approximately 100x and grown until OD600 ~0.1. at 27° C (roughly 2 doublings). Cells were then spun down (as above) and resuspended in media at 37° C and incubated at 37° C for 30 minutes before EdU was added to 10 uM final concentration. Cells were then further grown at 37° C for 90 minutes and either fixed with ethanol immediately (see below) or 37% formaldehyde was added to cultures to 3.7% final concentration and shaken at 37° C for 30 minutes. Cells were then spun down (as above) and washed in PBS twice.

Ethanol fixation, either alone or after formaldehyde fixation, was performed by spinning down cells (as above) and replacing PBS with approximately 1 mL 70% ethanol. Cells were vortexed until pellet dissolved. Cells were then spun down (as above) and washed twice with PBS, taking care to dissolve the pellet each time. EdU was ligated to Alexa-488 azide (Life Technologies) essentially as described by Hua and Kearsey *(30)* except that PBS buffer was used in place of TBS buffer. Note that formaldeyhyde fixation was required to preserve mCherry signal and ethanol fixation was required to perform the ``click'' reaction.

Agarose pad for imaging was created as described previously *(31)* except that two layers of frame seals (Biorad, SLF-1201) were placed on microscope slide to contain slab. Agarose pad was made from 2% low fluoresence agarose (Biorad, Catalog \#161-3100) in PBS (for spot counting) or YES media (for time-lapse movies). Cells were allowed to dry on agar pad for approximately 10 minute before a No 1.5 coverslip (VWR) was placed on top.

Microscopy

Microscopy was performed on a Nikon Eclipse Ti inverted microscope equipped with an Orca R2 (Hamamatsu) camera, a 100x Plan Apo oil objective (NA 1.40, Nikon), an automated stage (H117, Prior Scientific), and a Lumen 200 Pro metal arc lamp illumination system (Prior Scientific). Image acquisition was performed using microManager or microManager controlled by custom Matlab scripts. For time-lapse

imaging the microscope was encased in a custom-built incubator maintained at 30°C throughout the experiment. The following filter cubes (Semrock) were used for image acquisition: DAPI (excitation 390/40, dichroic 405, emission 452/45), GFP (excitation 472/30, dichroic 495, emission 520/35), YFP (excitation 500/24, dichroic 520, emission 542/27) and mCherry (excitation 562/40, dichroic 593, emission 641/75).

For spot detection, images for mCherry (mCherry filter) and SGI (YFP filter) and DAPI (DAPI filter) were taken in Z-stacks with 0.25 um spacing in a 6 um range with 200-300 ms exposure time. Brightfield images were taken at a single Z position that clearly showed the cell wall and any septum with 100ms exposure.

For timecourses, images were taken in mCherry and GFP channels in Z-stacks with 1.0 um spacing over 4 or 5 um range and 50 ms or 40 ms exposure in each channel. The percent of mitochondria in the smaller daughter was determined as the fraction of the total fluorescence in the mCherry channel that was in the smaller daughter. The fluorescence for each cell half was determined by first subtracting background and then adding pixel values from all Z-planes. A minority of cells with obvious mitochondrial photodamage (permanently balled, fragmented or aggregated mitochondria) were excluded from analysis.

Image Analysis

To count nucleoids in dividing cells, dividing cells were first identified by their straight and complete septa in bright field images and their outlines and septa traced using the microbeTracker *(32)* software for Matlab. Cells with incomplete or rounded septa were excluded from analysis as they had not divided or had been divided for more than 15 minutes (D. Huh, personal communication).

To identify nucleoids, custom Matlab (Mathworks, version 2013a) code was written to sharpen spots using a 3-dimensional unsharp mask (blurring ellipsoid was 3 pixels by 3 pixels by 1 pixel (xyz)). The sharpened image was then thresholded on the first local maximum of the entropy distribution of pixel intensities. The Matlab morphological commands bwmorph:clean, bwmorph:fill and imopen (with disk of radius 1) were then used on each slice. Connected areas in the 3D image (using the 6 neighbor definition) with fewer than 20 pixels were then eliminated. All other connected pixels were provisionally considered nucleoids. These identifications were confirmed by viewing the sharpened maximum projection of the image and manually correcting any missed or erroneously detected spots using the spotFinderM feature of microbeTracker. As spots had a broad range of intensities, the maximum projection of a log transformed version of the image was also checked for any missed spots and manually corrected. All code is available upon request.

MitoGraph

Mitograph software was used with the appropriate settings based the xy pixel size and the distance between images in the z plane. The surface-volume calculation was used

to estimate the volume of mitochondria in the cell. Cells where mitochondria were not correctly identified were excluded from data analysis.

Cell volume estimation

To estimate the available cytoplasmic volume in each cell half at division the nucleus was estimated to occupy 11% of the cytoplasm before division and equal sized nuclei were transported to each cell half, regardless of the sizes of the cells. Previous data report between 8% *(29)* and 12% *(33)* of the cell is composed of the nucleus. Using an average of these two estimates and that 10% of the cell is composed of cell wall *(33)* then roughly 11% of the cytoplasmic volume is occupied by the nucleus. Correcting for the occupied volume made the mitochondrial and nucleoid segregation fit the ``equal concentration" model even more accurately.

Relative absolute concentration differences between cells

To compute the concentration differences between daughter cells we used the following formula which normalizes the difference in concentration by the concentration of the cell before division. If l and r represent the number of nucleoids detected in the left and right cells respectively, V_l and V_r are the cytoplasmic volumes of the left and right cells, then the normalized concentration difference between the two cells is

$$\frac{\left| l/V_l - r/V_r \right|}{(l+r)/(V_l+V_r)}$$

Computing Distances between nucleoids

To calculate the distances between two nucleoids in the mitochondrial network, first, nucleoids were identified as previously described and computationally overlayed onto the network. Nucleoids were assigned to the point on the network with the nearest Euclidean distance. For this analysis mitochondria were considered 1-dimensional objects and two nucleoids were considered on the same edge if they were connected by unbranched mitochondria. Distances between nucleoids on unconnected mitochondria were not computed. Distances between nucleoids where the mitochondria between them was branched were also not computed. Only segments greater than 1um were considered as these are unlikely to be spurious artifacts of the image analysis. As the diffraction limit for the Alexa-488 was was 0.227 um, any nucleoids closer together than this distance were excluded.

For the computational ``random" model of nucleoid placement, 200 simulations were run exactly matching the number of nucleoids observed and the lengths of mitochondrial segments for each cell. Nucleoids were placed at a random position in unbranched mitochondrial segments longer than 1um match the analysis performed on the actual nucleoid data. The number of spots for each segment was Poisson distributed with average proportional to the length of the segment and the total number of nucleoids. To match the detection of the real spots, any simulated nucleoids closer together than 0.227 um were excluded from the simulated data as well.

Growth rate measurements

To measure growth rates for single cells a microfluidic device was constructed as in *(34)* but enlarged for pombe and modified to allow longer channels with even feeding to all cells.

The imaging conditions and microscopy were similar to *(34)* with some modifications. Cells were grown to OD600 ~ 0.4~0.6 in SC+PMG media at 32C, then loaded into the device. The device was connected to syringe filled with SC+PMG media, which was pumped by syringe pump at a speed of 20 uL/min, then was mounted onto a fluorescence microscope equipped with a custom incubator set at 32C. After waiting ~1 day to allow cells to adjust to a new environment, GFP, RFP, and bright field images were taken at appropriate intervals. Multiple Z planes were taken to cover 3~4um thick fission yeast. The typical experiment lasted for 3 days. Images were segmented and tracked with a custom written code in Matlab, and then manually verified. The conditions of growth were exceptionally uniform and had a coefficient of variation of only 2.76% over time, 2.45% between positions and 4.15% over the depth of the growth channel.

Plasmid construction

Plasmid pRJ06 was constructed using isothermal assembly of the PCR product of primers RJ-036 (5'-CAG GTG CCT TCG CTT TTC TTT AAG CAA GAG AAT TGT CGA GAT GGC CTC CAC TCG TGT CCT-3') and RJ-037 (5'-GAT GAT GGC CAT GTT ATC CTC CTC GCC CTT GCT CAC CAT GGA AGA GTA GGC GCG CTT CTG-3') on plasmid pYES-mtGFP (gift of B. Westermann *(35)* and primers RJ-034 (5'-ATG GTG AGC AAG GGC GAG G-3') and RJP-035 (5'-CTC GAC AAT TCT CTT GCT TAA AGA AAA GCG AAG G-3') on plasmid pDH92 (gift of D. Huh, unpublished). This plasmid was then cut with NotI and transformed into strain DH0 to make RJP005.

Plasmid pRJ26 was made from isothermal assembly of the the PCR product of primers RJ-037 and RJ-094 (5'-AAC ACG GGA TCC CCG GAT CC-3') on plasmid pRJ07 (unpublished) and primers RJ-034 and RJ-117 (5'-AAT TCC TGC AGG ATC CGG GGA TCC CGT GTT ATA TTA CCC TGT TAT CCC TAG CGG ATC TGC-3') on pDH62 (gift of D. Huh, unpublished). This plasmid was cut with MfeI and transformed into yFS284 to make RJP028.

Strain construction

PRP43-msfGFP translational fusions (for RJP041 and RJP042) were constructed by colony PCR of YJ014 with primers RJ-157 (5'-AGT GGA TTT TTC ATG CAA GTT GCC-3') and RJ-158 (5'-CAT ATT TTT GGC ATA AAG CTG CAC G-3') (~3.5 kB) and subsequently transformed into RJP005 to make RJP041 and RJP025 to make RJP042 with URA selection.

YJ014 was constructed by transforming the PCR product of msfGFP-ura4 (gift of D. Landgraf) flanked by ~300bp homologous sequences for prp43 following the protocol provided by Bahler et al. *(36)* The two homologous sequences H1/H2 were amplified

from purified DNA from DH0 using a pair of primers YJ014-f1 (5'-AGT GGA TTT TTC ATG CAA GTT GCC-3') and YJ014-r1 (5'-CCA GCA CCA GCA CCT GCT CCA CGT CGA GCG TTC TTT TTT GAT CTA G-3'), and a pair of YJ014-f2 (5'-GTT TAA ACG AGC TCG AAT TCA TCG AAA TCT AAT TTA CTG CTC GGT GAA TTA CAA ATA T-3') and YJ014-r2 (5'-CAT ATT TTT GGC ATA AAG CTG CAC G-3'), respectively. And then, msfGFP-ura4 flanked by the homologous sequences were amplified from pYJ003 and H1/H2 using primers of YJ014-f1 and YJ014-r2.

Strains and plasmids are available upon request.

Supplementary Text

Correspondence with previous measurements

As a further control of our nucleoid detection methods, we also compared our average measurements of nucleoid abundances to previous studies. In our assay newborn cells each inherited an average of 15.4 nucleoids or 18.3 accounting for the detection efficiency. Using previous estimates of the number of mtDNA genomes in newly divided *S. Pombe* cells at 100 genomes *(37)* this implies that each nucleoid contains roughly 5 genomes on average, within the range reported in other organisms by.

Detailed Explanation of CDF plots

In the CDFs of relative partitioning error of nucleoid segregation, the percent of total nucleoids in each cell half was subtracted from the percent of cytoplasmic volume in that cell half. The absolute value of these errors for both cell halves was summed to make the relative nucleoid segregation error for that cell. To calculate the errors for a model of randomly placed nucleoids in mitochondria, a binomial distribution of nucleoids in each cell half was created using the actual number of nucleoids and the actual split in the amount of mitochondria that was segregated to each cell half.

In Fig. S14, the CDFs of relative error of WT nucleoid segregation were computed as above. The errors for simulated spacings were created by simulating nucleoids on a single 1-d mitochondria according the the distributions in Figure 3C. The number of nucleoids and relative segregation of mitochondria was taken from the data of actual cells. 100 distributions each for 168 wild-type cells were performed assuming linear mitochondria that segregated as the observed wild-type cells did and randomly spaced nucleoids or nucleoids with observed spacing were then computationally placed in these mitochondria.

Mechanism of mitochondrial re-equilibration after initial separation

As shown in the main text, the mitochondria re-equilibrate throughout the cell before division. To further understand the mechanism behind this re-equilibration after initially segregating with the nucleus, we observed cells in which both the mitochondria and tubulin were tagged with fluorescent proteins (MYP101 cells). We observed that the mitochondria moved to the cell poles with the ends of the spindle but with a less clear phenotype than cells without atb1-GFP. This may be an effect from the disruptive GFP

tag even though it was transiently induced in addition to the untagged copy. Mitochondria were released from the poles before or during spindle dis-assembly in roughly half the cells. Thus spindle dis-assembly does not appear to be necessary for release of mitochondria from the poles.

In cells for which we can clearly score a marked release from the poles, 13 out of 15 released their mitochondria from the poles after or during the formation of new microtubules independent of the spindle. In addition mitochondria immediately colocated with these new microtubules, suggesting that the formation of new microtubules just before division enable re-equilibration of mitochondria.

We also watched the process of mitochondrial re-equilibration in strains in which the Mmb1 protein had been deleted (RJP044). In all cells observed (n=13), the mitochondria still transiently localized to the poles of cells, indicating that Mmb1p is not required for mitochondria to associate with the poles. Instructively, we observed one cell in which all the mitochondria was present on one side of the cell and did not move to the other side even after the nuclei had been separated (Fig S3B). Combined these observations suggest that mitochondria associate with the poles independent of Mmb1p and are re-equilibrate when the microtubule network is reformed. Full re-equilibration of mitochondria throughout the cell seems to require Mmb1p so that mitochondria can associate with these newly formed microtubules that span both halves of the cell just before division.

Yeast strains

All strains were based on the *S. Pombe* strain FWP172 (a gift of F. Winston) except for PHP14 (a gift of T. Fox). Deletions were constructed using standard PCR mediated techniques or PCR techniques based on the *S. Pombe* deletion collection *(38)*.

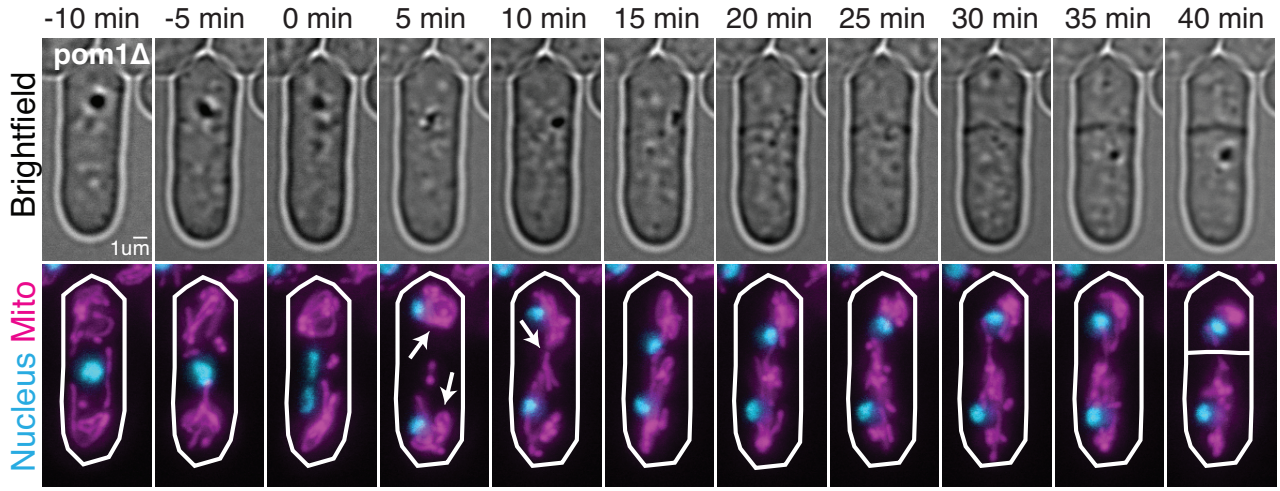

Fig. S1

Timelapse images of a dividing *pom1Δ* cell (RJP042) in brightfield and with mitochondrial matrix-targted mCherry (magenta) and GFP labeled nuclei (cyan). Arrows at 5 min indicate initial separation of mitochondria at the same time as nuclei and then

reformation of a continuous mitochondrial network at 10 min but before division (40 min). Scale bars indicate 1um.

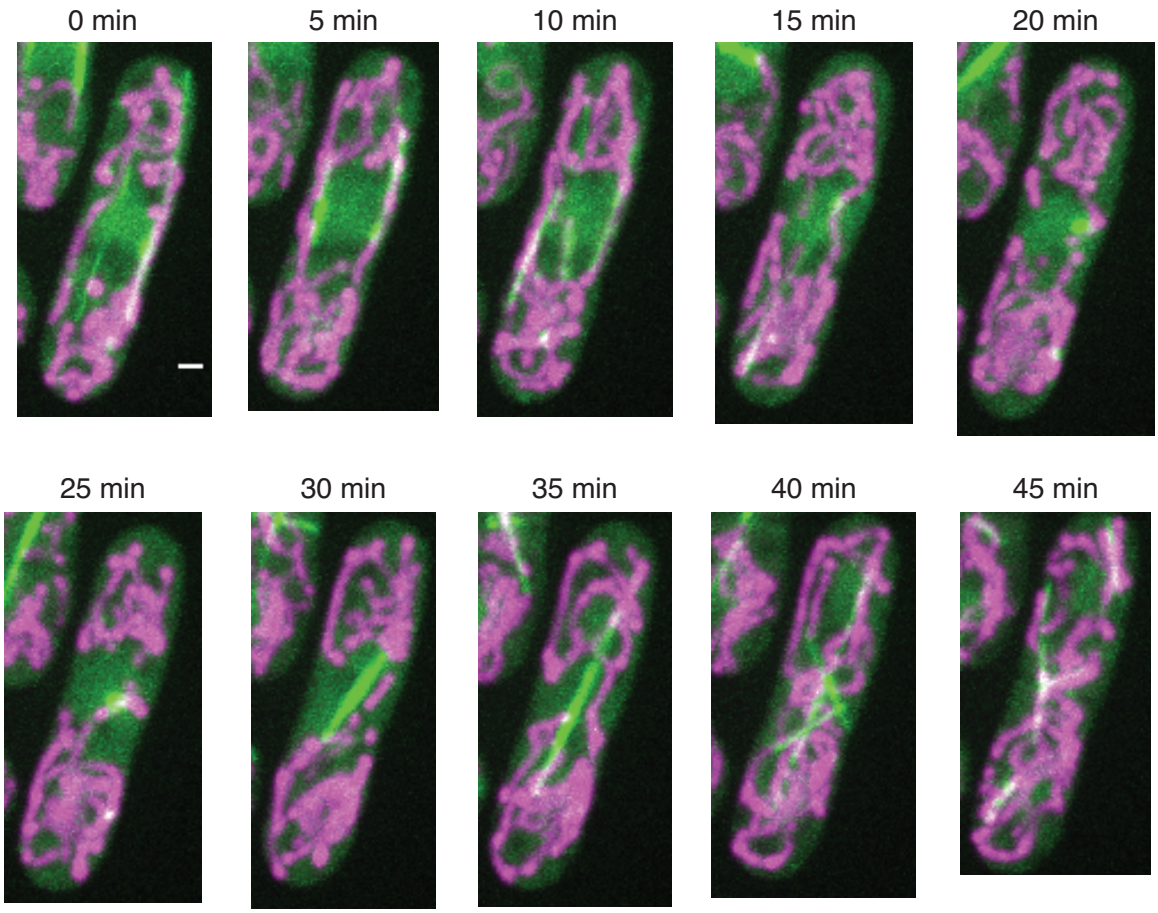

Fig. S2

Timelapse maximum projection images of a cell (MYP101) with the Cox4 leader peptide fused to DsRed (magenta) showing the mitochondria and atb1-GFP (green) showing the microtubules and spindle. Cells were grown in Edinburgh Minimal Media overnight to induce nmt1 promoters. The time lapse shows that the mitochondrial network reforms as the spindle disintegrates and individual microtubules are formed (see images at 40 min and 45 min).

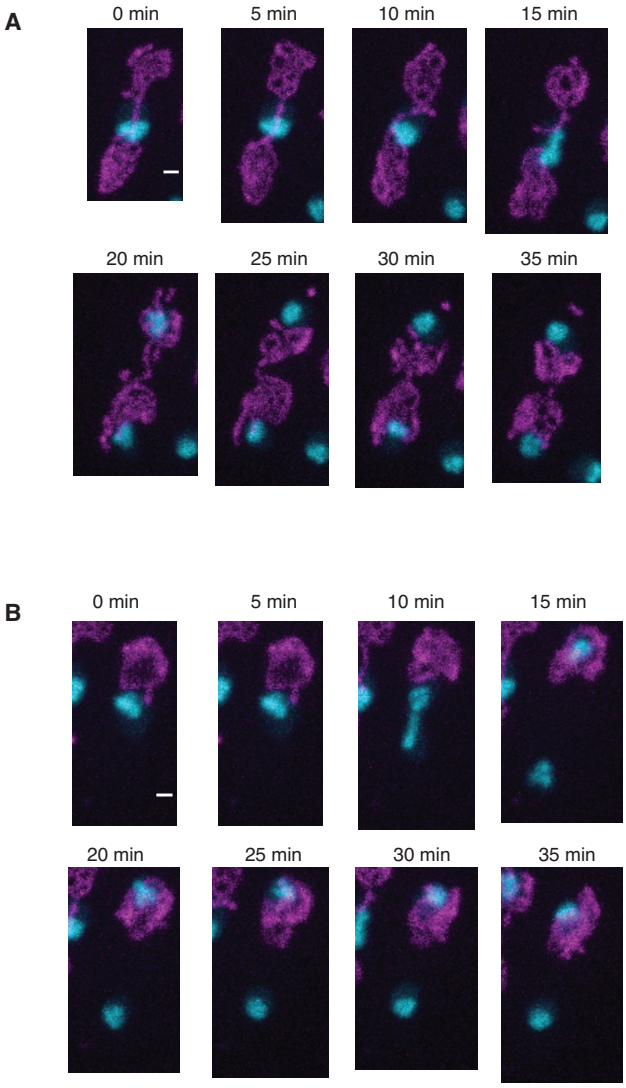

Fig. S3

(A) and (B) Timelapse maximum projection images of a *mmb1Δ* cell (RJP044) with both the mitochondria (magenta) and the nucleus (cyan) labeled. The cell in (B) divides with no mitochondria the bottom daughter cell.

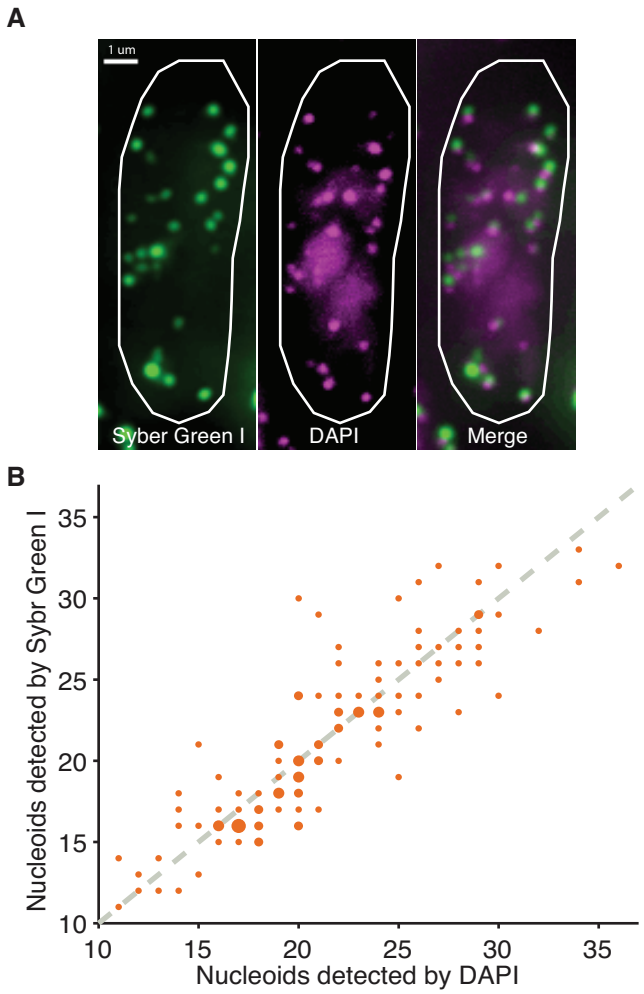

Fig. S4

Quantification of mitochondrial nucleoids with fluorescent dyes **(A)** Sample images of an *S. Pombe* cell stained with Sybr Green I (green) and DAPI (magenta). The outline of the cell is provided for reference. Note that the overlay between SGI and DAPI spots is not exact and that slight offsets are seen in the overlay because the spots moved slightly between acquisition of each image. Scale bar is 1um. **(B)** The number of nucleoids detected with SGI or DAPI in each cell is plotted. The area of each point is proportional to the number of samples observed. The dashed gray line indicates equality between the two methods. (n=116 cells (RJP005)). To detect and count spots, automated image analysis followed by manual correction was performed (see methods).

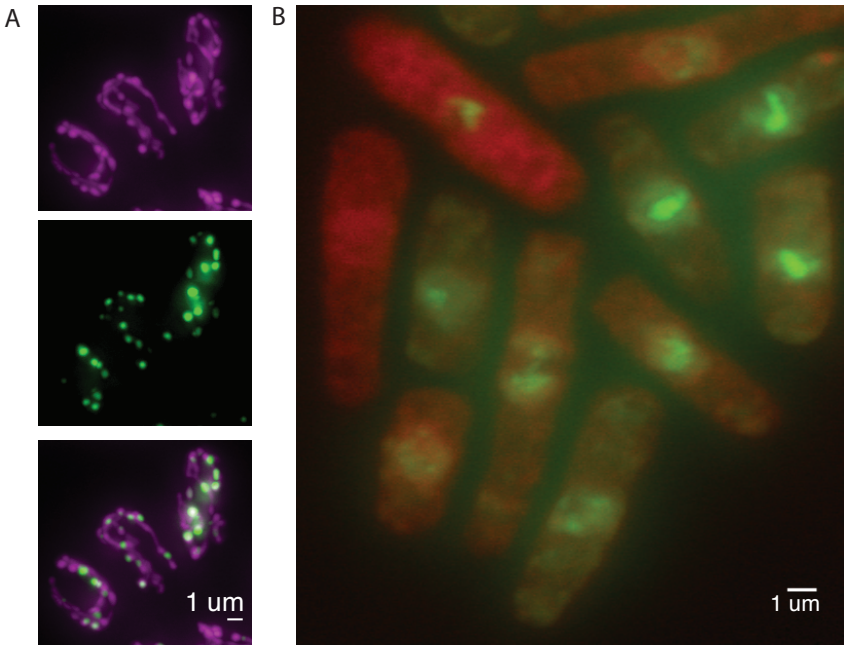

Fig. S5

Sybr Green I staining is specific to mitochondrial nucleoids. **(A)** RJP005 imaged with Top: Mitochondrially localized mCherry (magenta), Middle: Sybr Green I staining (green). Bottom: overlay. Note that SGI staining was used to determine the number of nucleoids in each cell but the location and morphology of the mitochondria and nucleoids were disturbed. **(B)** ρ^0 cells (PHP14) stained with Sybr Green I (green) and autofluoresence in mCherry channel (red). Only nucleus and no mitochondrial nucleoids are visible.

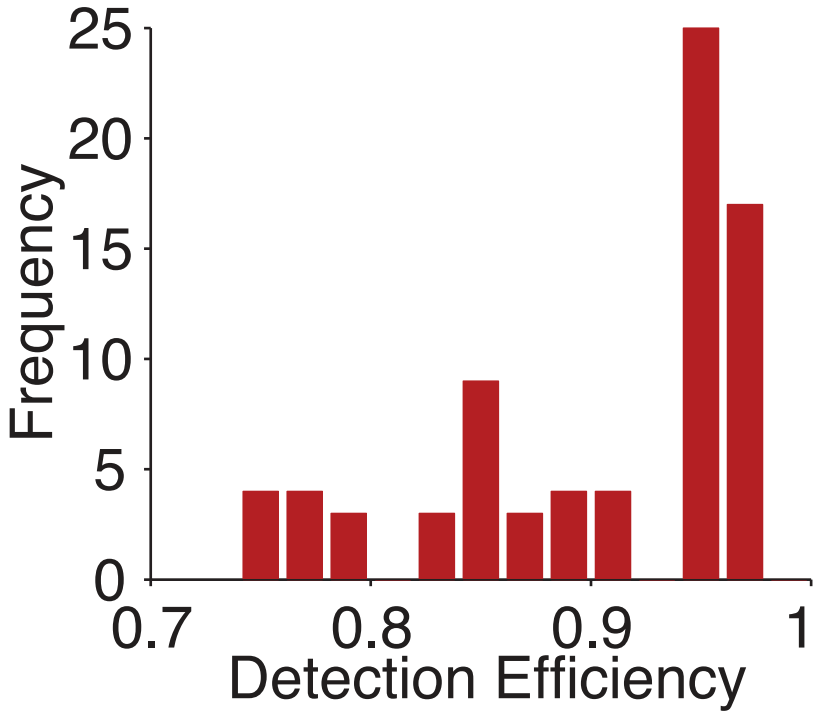

Fig. S6

Histogram of detection efficiencies calculated by using the variability in detection between SGI and DAPI and assuming a binomial model of nucleoid detection. (See methods for details on calculation.)

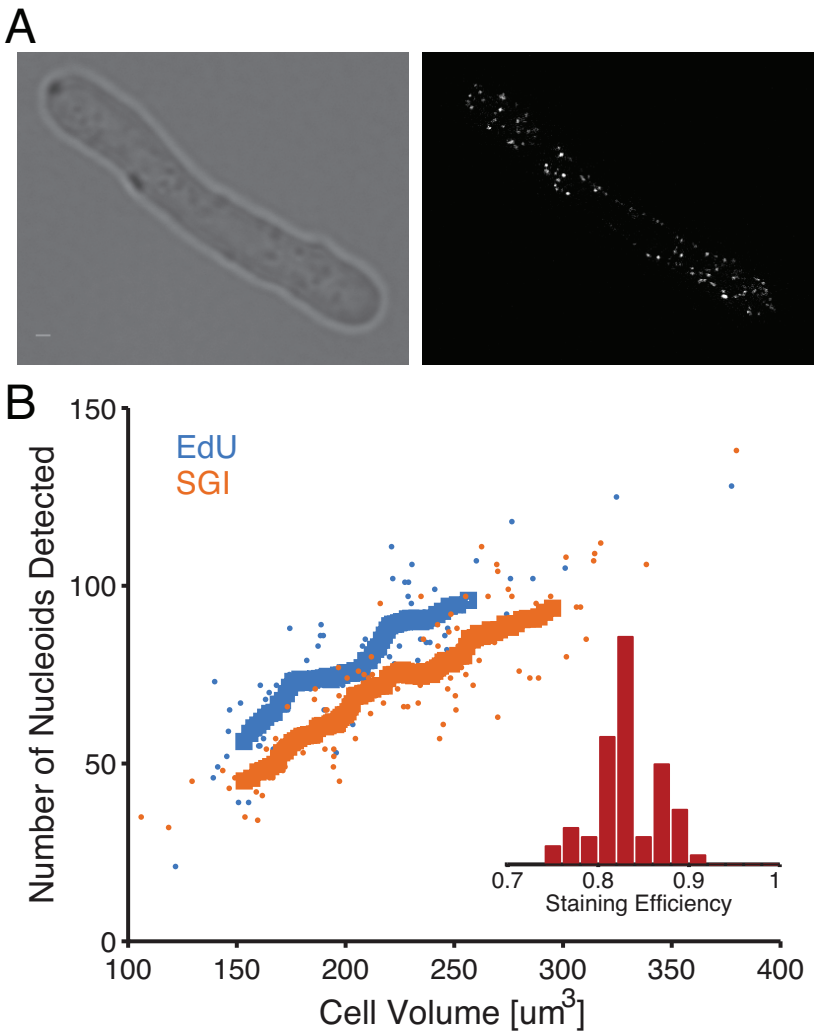

Fig. S7

EdU staining provides orthogonal method to verify Sybr Green I staining efficiency. **(A)** A yeast strain (ySF284) was arrested in G2, allowed to incorporated EdU, fixed and Alexa-488 azide was ligated to EdU with ``click" chemistry (see methods). Left: Brightfield image of cell, Right: Alexa-488 channel visualizing nucleoids. **(B)** The number of nucleoids detected by SGI and EdU plotted against cell volume. Thick lines are running average of 20 cells. Inset: histogram of calculated efficiency of SGI vs EdU. To calculate efficiency, the running average of nucleoids identified by SGI was compared to the running average of nucleoids identified by EdU. For each point in the running average of SGI, the cell volume was noted and a matching cell volume from the running average of EdU cells was chosen for comparison. If there was no exact match in cell volume, a linear interpolation from the two points closest in volume was used. (n=77 cells for EdU and n=108 cells for SGI).

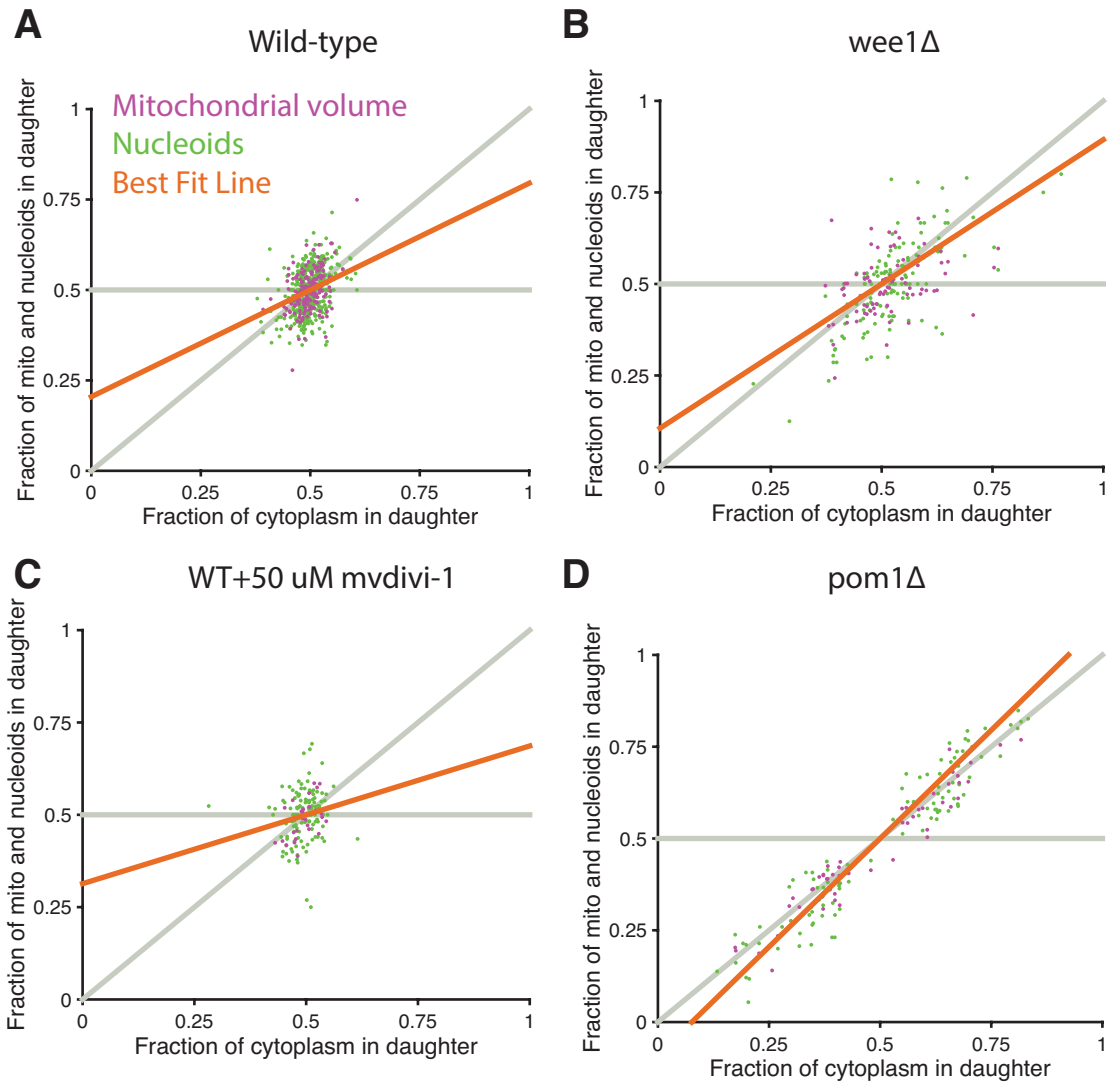

Fig. S8

Analysis of mitochondrial volume and nucleoid distribution to daughter cells for (A) WT (172 cells for mitochondrial volume, 421 cells for nucleoids) (B) *wee1Δ* (77 cells for mitochondrial volume, 132 cells for nucleoids), (C) cells treated with the mitochondrial fission inhibitor mdivi-1 (128 cells with mitochondrial volume) and (D) *pom1Δ* cells as shown in Fig 1D (nucleoids, 102 cells, mitochondrial volume, 52 cells).

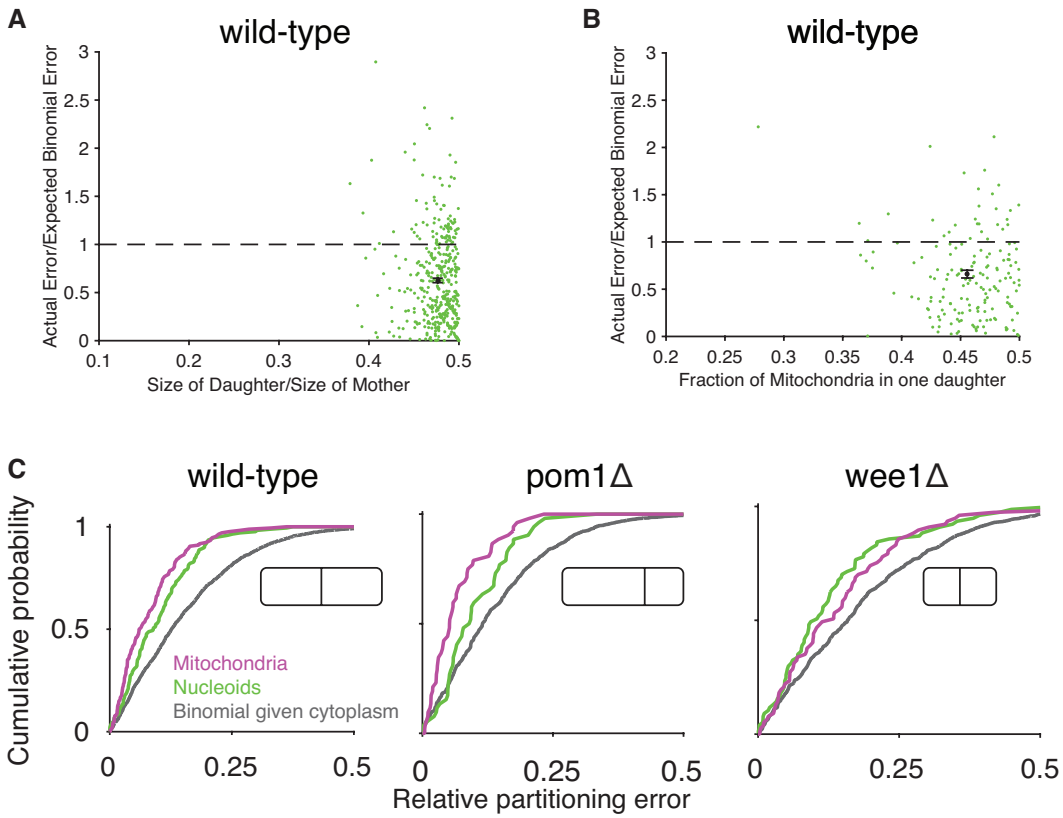

Fig. S9

(A) Nucleoid segregation error normalized to a binomial model taking into account cell division asymmetry plotted against the degree of asymmetric cell division in wild-type cells. **(B)** Nucleoid segregation error normalized to a binomial model based on mitochondrial segregation plotted against the degree of asymmetric mitochondrial division in wild-type cells. For (A) and (B), only the daughter with the smaller fraction is shown; the green points are individual cells and the black point is their average; error bars indicate s.e.m. **(C)** Cumulative distribution functions (CDFs) of the relative partitioning errors of mitochondrial volume (magenta) and nucleoid partitioning (green) compared to cytoplasmic partitioning for wild-type (RJP005, n=168 cells), *pom1Δ* (RJP025, n=52 cells), and *wee1Δ* (RJP029, n=77 cells). Mitochondria and nucleoids were more accurately partitioned than the binomial model would predict (t-test, Nucleoids: wild-type: $p<10^{-15}$, *pom1Δ*: $p<10^{-3}$, and *wee1Δ* : $p<10^{-3}$); mitochondria: wild-type: $p<10^{-27}$, *pom1Δ*: $p<10^{-11}$, and *wee1Δ* : $p<10^{-2}$).

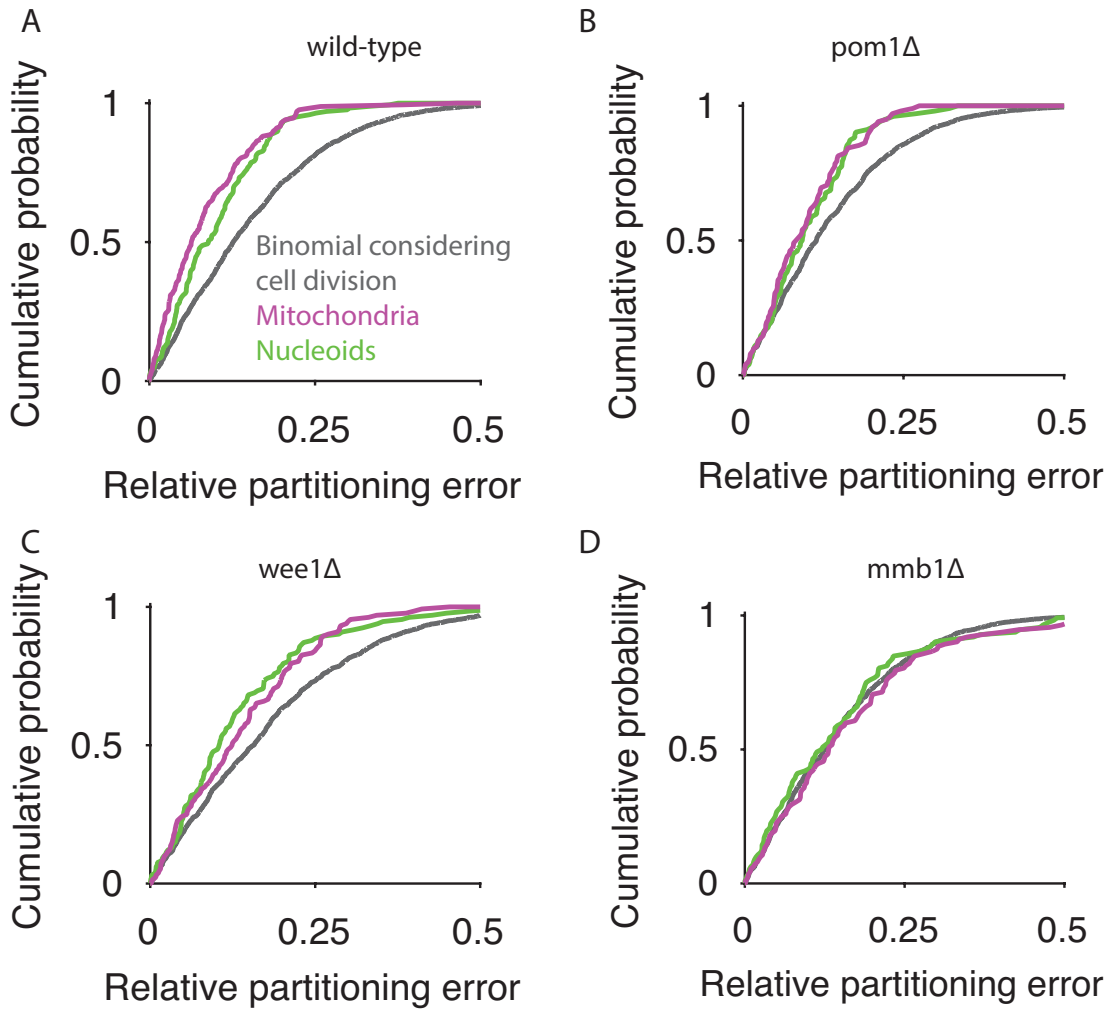

Fig. S10

Cumulative distribution functions (CDFs) of the relative partitioning errors but with total fluorescence in the mcherry channel instead of extracted mitochondrial volume. Nucleoid partitioning (green) is also shown.compared to cytoplasmic partitioning for (A) wild-type (RJP005, n=168 cells), (B) *pom1Δ* (RJP025, n=102 cells), (C) *wee1Δ* (RJP029, n=132 cells) and (D) *mmb1Δ* (RJP029, n=112 cells). Mitochondria and nucleoids were more accurately partitioned than the binomial model would predict in all cells except *mmb1Δ* cells (t-test, mitochondria: wild-type: $p<10^{-23}$, *pom1Δ*: $p<10^{-7}$, *wee1Δ* : $p<10^{-5}$ and *mmb1Δ* p=0.90).

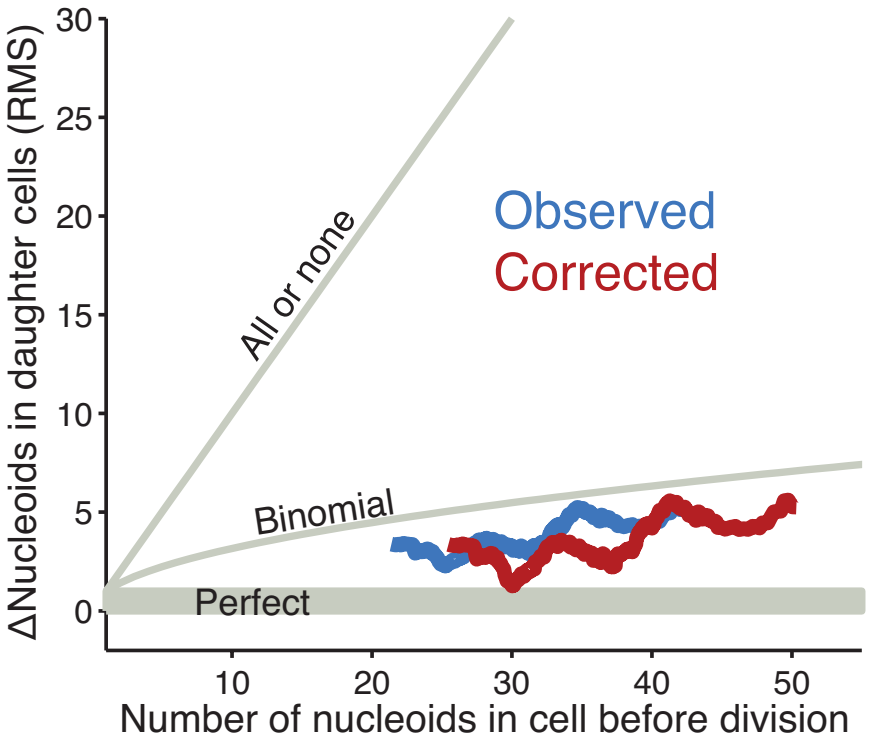

Fig. S11

Correcting for random undercounting of nucleoids shows that wild-type cells partition even more accurately than observed. A running average (50 points) of the root mean square (RMS) error between wild-type daughter cells is plotted against the total number of nucleoids in the cell before division (blue). The corrected version (red) shifts to the right to correct for 84% undercounting of nucleoids. The line moves down because random undercounting is a binomial process and undoing this, shifts the trend away from the binomial line. See methods and Huh and Paulsson *(22)* for details.

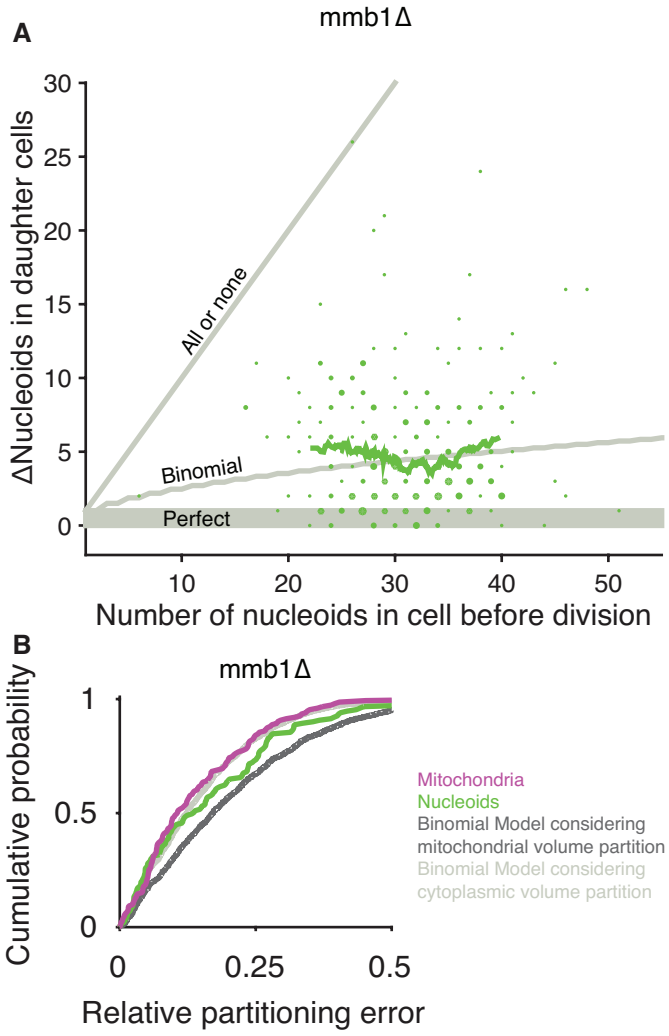

Fig. S12

(A) Analysis of nucleoid segregation to daughter cells for *mmb1Δ* cells (n=277) with size of point representing the number of cells observed. 20% of cells segregated perfectly, 44% segregated worse than binomial and the rest fell between perfect and binomial. The running average of 50 cells plotted as a line. **(B)** CDFs of partitioning errors for mitochondrial volume and nucleoid segregation in *mmb1Δ* cells and a binomial models of considering cytoplasmic volume partition and considering mitochondrial volume partitioning. The mean nucleoid segregation error for *mmb1Δ* cells is larger than a binomial model only considering its cytoplasmic segregation but not significantly so (t-test, p=0.035). However, it is significantly less than a binomial model considering its mitochondrial volume partition (t-test, p=.0015)

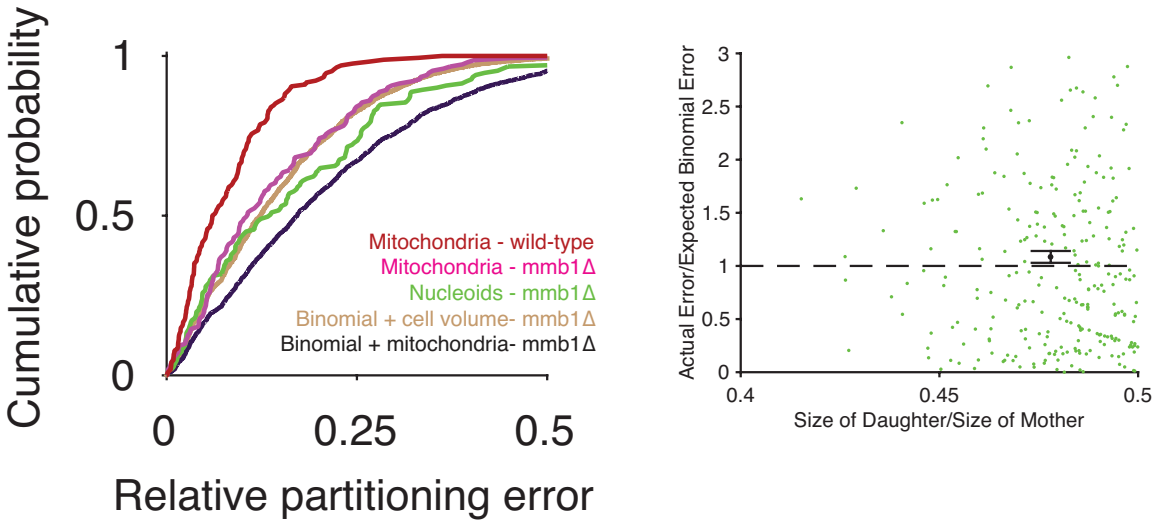

Fig. S13

(A) Cumulative probability distributions of *mmb1Δ* strains with wildtype and binomial models for comparison.``Binomial + cell volume" refers to a model where the nucleoids are independently assorted to daughter cells in proportion to their cell volumes. ``Binomial + mitochondria" refers to a model where the nucleoids are independently assorted to daughter cells in proportion to their mitochondrial volumes. **(B)** The ratio of the actual segregation error to the average expected binomial error vs. the relative size of the daughter cell is plotted for each dividing cell in an *mmb1Δ* strain. The smaller of the two sister cells was chosen to plot. The average and s.e.m. of these cells is also plotted.

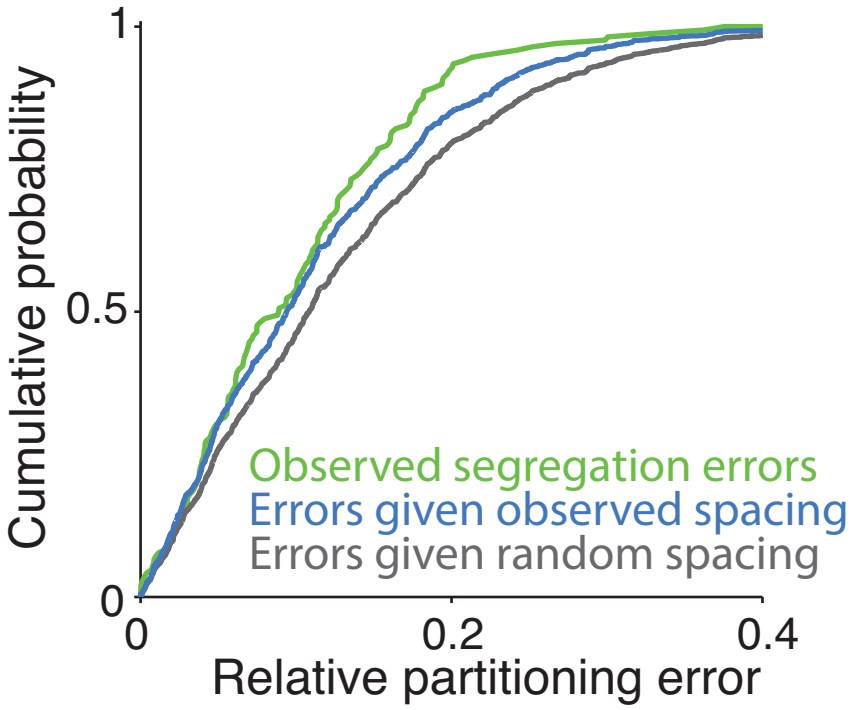

Fig. S14

CDF of relative nucleoid segregation errors for wild-type cells, the observed nucleoid spacing (blue) and random spacing (gray). The random spacing model segregates nucleoids with more error than wild-type segregation (t-test, $p<10^{-6}$). Modeling the observed spacing creates segregation that is not distinguishable from the observed wild-type segregation (t test, $p=0.02$).

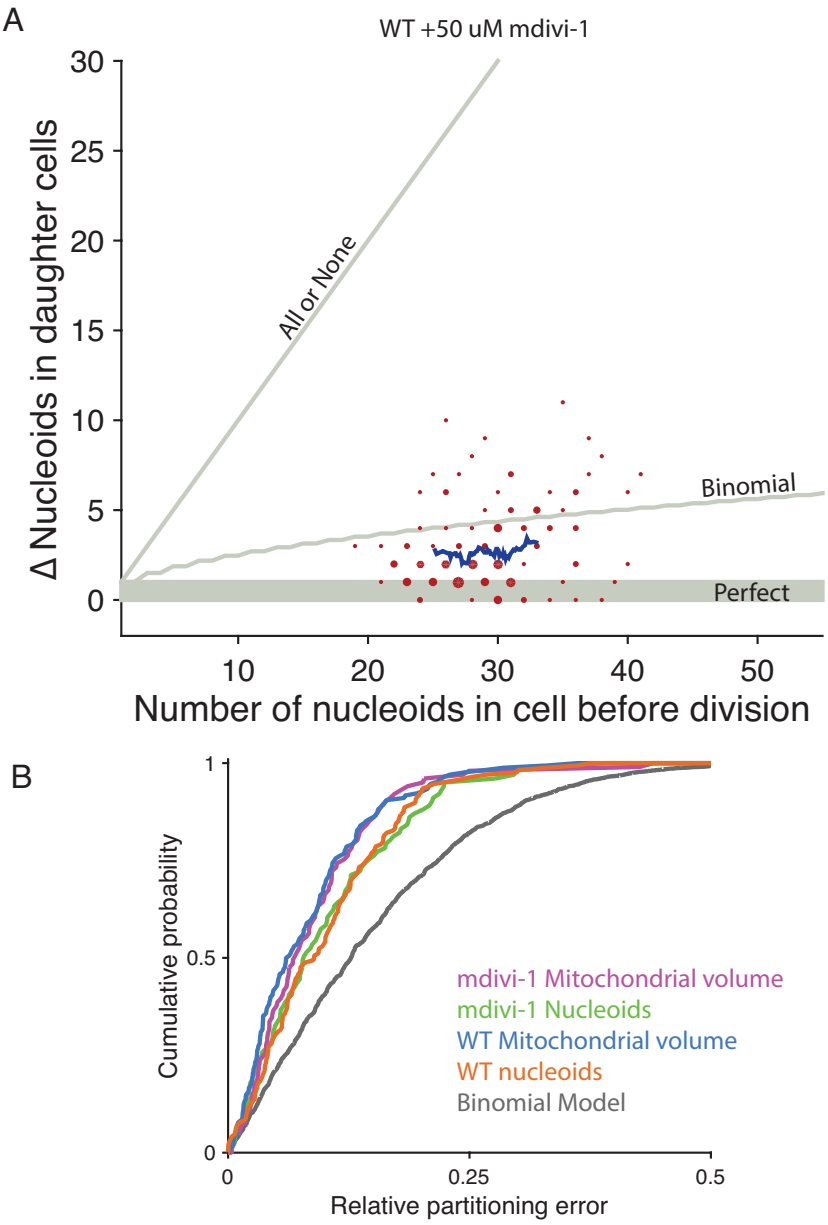

Fig. S15

(A) Absolute error of nucleoid segregation in cells treated with 50 uM mdivi-1 for greater than 4 hours in YES media. Size of points indicates number of cells (128 cells total). Blue line is running average for 25 cells. **(B)** CDFs of partitioning errors for mitochondrial volume and nucleoid segregation in WT cells treated with mdivi-1 cells in comparison with untreated cells and a binomial model. The mean partitioning errors for cells treated with mdivi-1 were not significantly different than the untreated cells for both nucleoids and mitochondrial volume.

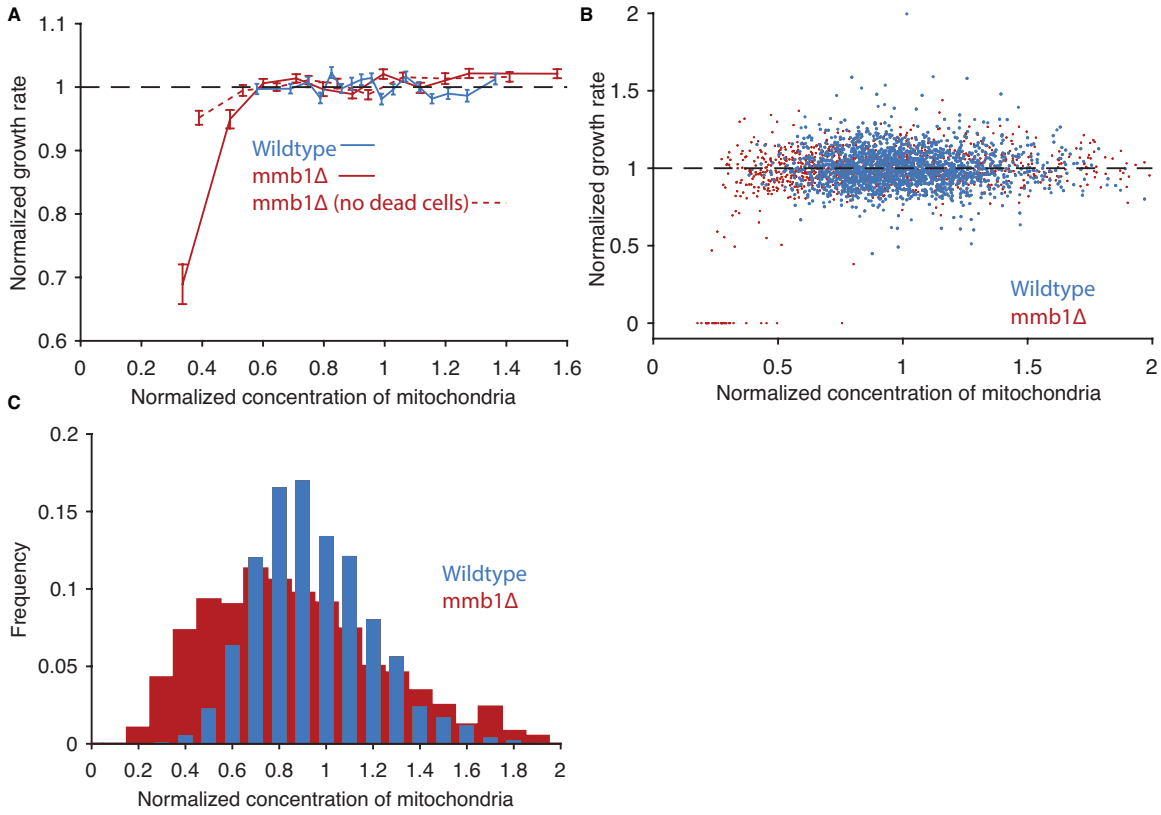

Fig. S16

(A) The normalized growth rate of cells is plotted against the normalized concentration of mitochondria for both WT and *mmb1Δ* cells. Each point is an average of 200 data points and error bars are s.e.m. as in Figure 4C of the main text. **(B)** Actual data points for part (A) and for Fig. 4D of the main text. **(C)** A histogram of the normalized concentration of mitochondria WT and *mmb1Δ* strains. In all panels for this figure and figure 4D of main text the growth rates are normalized to the mean of all growing cells of that strain. The actual doubling times for WT cells was 189 min and for *mmb1Δ* cells was 198 minutes (for cells with finite division times). The two distributions of mitochondria are further normalized against each other using the difference in mean mitochondrial concentration from the MitoGraph calculations: WT had 7.4% more mitochondria than the *mmb1Δ* strain on average.

Table S1.
Strains used in this study.

Name	Genotype	Source
DH0	ade6::ade6+ ura4-D18 leu1-32 ade6-m210 h-	D. Huh
yFS284	ura4-D18 his7-366 cdc25-22 leu1::pFS181(leu1+ adh1:hENT1) pJL218(his7+ adh1:tk) (integrated at random position)	N. Rhind
PHP14	ade6-M216, leu1-32, ptp1-1, ρ^0	T. Fox
DH60	leu1::Padh1-GST-NES-mCherry-leu4+ leu1-32 ura4-D18 h-	D. Huh
RJP005	ura4-D18 leu1-32:pRJ06(leu+:adh1pr:mtmCherry)	This Study
RJP016	ura4-D18 leu1-32:pRJ06(leu+:adh1pr:mtmCherry) mmb1Δ::kanMX4	This Study
RJP025	ura4-D18 leu1-32:pRJ06 (leu+:adh1pr:mtmCherry), pom1Δ::kanMX	This Study
DH132	qcr7-mGFPmut3 leu1::Padh1-GST-NES-mCherry-leu1+ leu1-32 ura4-D18 h-	This Study
YJ053	qcr7-mGFPmut3 leu1::Padh1-GST-NES-mCherry-leu1+ leu1-32 ura4-D18 h- mmb1Δ::kanMX4	This Study
DH128	isu1-mGFPmut3 leu1::Padh1-GST-NES-mCherry-leu1+ leu1-32 ura4-D18 h-	This Study
DH134	sod1-mGFPmut3 leu1::Padh1-GST-NES-mCherry-leu1+ leu1-32 ura4-D18 h-	This Study
YJ72	shm2-mGFPmut3 leu1::Padh1-GST-NES-mCherry-leu1+ leu1-32 ura4-D18 h-	This Study
RJP028	ura4-D18 his7-366 cdc25-22 leu1::pFS181(leu1+ adh1:hENT1) pJL218 integrated (his7+ adh1:tk), pRJ26 integrated (pADH1-MLS-mcherry)	This Study
RJP029	ura4-D18 leu+:pRJ06 (leu+:adh1pr:mtmCherry), wee1Δ::KanMX6	This Study
RJP029	ura4-D18 leu+:pRJ06 (leu+:adh1pr:mtmCherry), wee1Δ::KanMX6	This Study
MYP101 (RJP037)	h+ nmt1-preCox4-DsRed::leu1+ nmt1-atb1-GFP::LEU2 ade6-M216 ura4-D18 leu1-32	I. Tolic
RJP041	ura4-D18 leu1-32:pRJ06 (leu+:adh1pr:mtmCherry), prp43:msfGFP:URA4	This Study
RJP042	ura4-D18 leu1-32:pRJ06 (leu+:adh1pr:mtmCherry), pom1Δ::kanMX, prp43:msfGFP:URA4	This Study
YJ014	prp43-msfGFP-ura4+, leu1::Padh1-GST-NES-mCherry-leu4+ leu1-32 ura4-D18 h-	This Study
RJP044	ura4-D18 leu+:pRJ06 (leu+:adh1pr:mtmCherry), prp43:mGFPmut3:URA4, mmb1::kanMX4	This Study